

Barycentric-alignment and invertibility for domain generalization

Boyang Lyu¹, Thuan Nguyen^{1,3}, Prakash Ishwar², Matthias Scheutz³, Shuchin Aeron¹ *

February 3, 2022

Abstract

We revisit Domain Generalization (DG) problem, where the hypotheses are composed of a common representation mapping followed by a labeling function. Popular DG methods optimize a well-known upper bound to the risk in the unseen domain. However, the bound contains a term that is not optimized due to its dual dependence on the representation mapping and the unknown optimal labeling function for the unseen domain. We derive a new upper bound free of terms having such dual dependence by imposing mild assumptions on the loss function and an invertibility requirement on the representation map when restricted to the low-dimensional data manifold. The derivation leverages old and recent *transport inequalities* that link optimal transport metrics with information-theoretic measures. Our bound motivates a new algorithm for DG comprising Wasserstein-2 barycenter cost for feature alignment and mutual information or autoencoders for enforcing approximate invertibility. Experiments on several datasets demonstrate superior performance compared to the state-of-the-art DG algorithms.

1 INTRODUCTION

In many real-world applications of modern machine learning, the training (seen) data and the test (unseen) data may belong to different *domains*, leading to the loss of predictive power of the learned models. For example, a model trained on data from one hospital may not work well when the test data is from another hospital [Gulrajani and Lopez-Paz, 2021], a drowsiness driving estimator trained on one group of subjects does not generalize well for other subjects [Cui et al., 2019], a cognitive workload estimator from fNIRS (functional near-infrared spectroscopy) measurements may not generalize well across sessions and subjects [Lyu et al., 2021].

These types of problems are broadly classified into two categories, viz., Domain Adaptation (DA) [Ben-David et al., 2007] and Domain Generalization (DG) [Blanchard et al., 2011]. Both DA and DG aim to find a model that can generalize well when the seen domain training data does not share the same distribution as the testing data from the unseen domain. The key difference between DA and DG is that DA allows access to the (unlabeled) unseen domain data during the training process while DG does not, leading to a more challenging problem. Both DG and DA have a close relationship with

^{*1} - Tufts University, Dept. of ECE, ² - Boston University, Dept. of ECE, ³ - Tufts University, Dept of CS.
Corresponding authors: Boyang Lyu, email: Boyang.Lyu@tufts.edu.

Transfer Learning Wang et al. [2021], all of which aim to enhance the robustness of the learned model. For an extensive survey and related literature, we refer the reader to excellent recent surveys [Wang et al., 2021, Zhou et al., 2021b].

To address the problem of DG, motivated by the seminal works of Ben-David et al. [2007, 2010], one usually parameterizes the hypothesis as composed of a representation function followed by a labeling function [Albuquerque et al., 2019, Dou et al., 2019, Li et al., 2018a, Zhou et al., 2021a]. The essential insight from the upper bound derived in [Ben-David et al., 2007, 2010] is that the risk on the unseen domain is upper bounded by three terms: (1) the prediction risk on the mixture of seen domains, (2) discrepancy or divergence between the data distributions in the representation space, and (3) a *combined risk* across all domains that is implicitly dependent on both the representation map and the unknown optimal labeling function from the unseen domain. Due to this dual dependency, most existing works ignore optimizing the third term (*combined risk*) and treat it as a constant for a given representation map. Ignoring the *combined risk*, a large body of the DG (as well as DA) methods [Li et al., 2018a, Ganin et al., 2016, Zhao et al., 2019] are essentially based on a variation of the following theme - learn a domain invariant representation mapping *or* align the domains in the representation space, together with learning a common labeling function controlling the prediction loss across the seen domains. However, it is worth noticing that the *combined risk* is actually a function of the representation map and hence needs to be part of the optimization. A detailed analysis of the shortcomings of the previous studies is provided in our Appendix A.1.

1.1 Main Contributions

To address the shortcoming discussed above, we first make a mild assumption that the class of representation mappings is (nearly) invertible when restricted to distributions that lie on low-dimensional manifolds, well-known as the manifold hypothesis [Lei et al., 2020]. Under this assumption, we derive a new upper bound for the risk in the representation space comprising three terms: (1) the prediction risk across seen domains in the input space; (2) the discrepancy/divergence between the induced distributions of seen and unseen domains in representation space that can be expressed in terms of the Wasserstein-2 Barycenter [Santambrogio, 2015] of the seen domains. For this, we leverage old and new *transport inequalities*, which also help avoid an additional Lipschitz assumption on the loss function that is typically assumed in related works; and (3) a *combined risk* term that is a constant with respect to the representation map and the labeling function to be learned. A detailed comparison between previous bounds and our work can be found in Appendix A.1.

Our (manifold-restricted) invertibility assumption provides a natural justification for the use of an auto-encoder-like mechanism, which to date had been heuristically motivated in [Li et al., 2018a, Ghifary et al., 2015]. Moreover, to avoid introducing additional parameters to train for, namely the decoder, we propose the use of mutual information between the data and the representation as a surrogate for enforcing the approximate invertibility of the representation map. It may appear that having both invertibility and alignment is counter-intuitive but note that the alignment requirement does not preclude invertibility and vice-versa. Indeed, there are infinitely many (manifold-restricted)

invertible maps for any given data manifold, and there could exist one which can align several domains simultaneously. Even though the results in this paper are mainly based on the assumption of invertibility of representation maps, we relax this assumption to approximate invertibility but with some additional technical conditions as discussed in Appendix B.2.

Finally, based on these theoretical insights, we propose two novel algorithms: Wasserstein Barycenter Auto-Encoder (WBAE) and Wasserstein Barycenter Mutual Information (WBMI). The proposed algorithms leverage recent advances in the fast and efficient computation of Wasserstein barycenters and advances in reliable gradients of mutual information estimation. We also note that the proposed algorithms bypass the adversarial mechanism for domain alignment in the representation space.

1.2 Related Work

Our work is closely related to the work that aims to learn the domain invariant features by decomposing the prediction function into a representation function followed by a classifier. For example, in [Albuquerque et al., 2019], the authors propose a model consisting of three parts: a feature extractor, a classifier, and domain discriminators. The feature extractor learns the task-sensitive but domain-invariant features via minimizing the cross-entropy loss w.r.t the task label and maximizing the sum of domain discriminator loss. The domain discriminator loss is treated as an estimation of \mathcal{H} divergence between all seen domains [Ben-David et al., 2010], which has its roots in the works Ganin et al. [2016], Li et al. [2018b] from the Domain Adaptation area. Following a similar idea, Li et al. [2018a] aligns the representation distributions from different domains via minimizing their maximum mean discrepancy. In Dou et al. [2019], the authors adopt a gradient-based episodic training scheme for DG, the extracted features are enforced to keep the global class relationship and the local task-related clusters via minimization of alignment loss between soft-confusion matrices and contrastive loss. Arjovsky et al. [2019] propose Invariant Risk Minimization algorithm to learn features such that the optimal classifiers on top are matched across domains. Nam et al. [2021] consider different styles of different domains as the main factor causing the domain gap, and achieve DG by disentangling it from learned features. Among the large body of works on the DG problem, we consider Blanchard et al. [2021], Ganin et al. [2016], Krueger et al. [2021], Li et al. [2018b], Arjovsky et al. [2019] as recent exemplars of principled algorithms guided by theory and we mainly focus on comparing the performance of our methods against methods from these papers.

Since our proposed upper bound is based on the Wasserstein distance, it is worth mentioning the work proposed in Redko et al. [2017], Shen et al. [2018], Zhou et al. [2021a]. Specifically, Zhou et al. [2021a] use the pairwise Wasserstein-1 distance [Peyré and Cuturi, 2019, Santambrogio, 2015] to estimate the divergence between different seen domains. Using the dual form of the Wasserstein-1 distance, the feature extractor in Zhou et al. [2021a] minimizes a combination of cross-entropy loss, Wasserstein distance loss, and a contrastive loss to achieve DG. On the other hand, [Redko et al., 2017, Shen et al., 2018] are designed for DA problem and constructed based on the Wasserstein-1 distance. Even though the bounds from [Redko et al., 2017, Shen et al., 2018] share some similarities with ours, their bounds are on the input space and do not explicitly motivate the use of representation functions.

In addition, their approaches also require more assumptions than our approach, which will be discussed later in Section 2.1.

2 THEORETICAL ANALYSIS AND PROPOSED METHODS

We consider a *domain* v as a triple $(\mu^{(v)}, f^{(v)}, g^{(v)})$ consisting of a distribution $\mu^{(v)}$ on the inputs $\mathbf{x} \in \mathbb{R}^d$, a representation function $f^{(v)} : \mathbb{R}^d \rightarrow \mathbb{R}^{d'}$ where $d' \leq d$, and a stochastic labeling function $g^{(v)} : \mathbb{R}^{d'} \rightarrow \mathcal{Y}$ mapping the representation space to label space \mathcal{Y} . We denote the unseen domain by $(\mu^{(u)}, f^{(u)}, g^{(u)})$ and the S seen domains by $(\mu^{(s)}, f^{(s)}, g^{(s)})$, $s = 1, \dots, S$.

Let $\mathcal{F} = \{f | f : \mathbb{R}^d \rightarrow \mathbb{R}^{d'}\}$ be a set of *representation functions*, $\mathcal{G} = \{g | g : \mathbb{R}^{d'} \rightarrow \mathcal{Y}\}$ a set of stochastic *labeling functions*, and $\mathcal{H} := \mathcal{G} \circ \mathcal{F}$ the set of *hypothesis* $h : \mathbb{R}^d \rightarrow \mathcal{Y}$ obtained by composing each $g \in \mathcal{G}$ with each $f \in \mathcal{F}$, i.e., $h = g \circ f$.

Define the risk of using a hypothesis h in domain v by:

$$R^{(v)}(h) := \mathbb{E}_{\mathbf{x} \sim \mu^{(v)}} [\ell(h(\mathbf{x}), h^{(v)}(\mathbf{x}))] \quad (1)$$

where $\mathbb{E}[\cdot]$ denotes expectation, $h^{(v)} = g^{(v)} \circ f^{(v)}$, and $\ell(\cdot, \cdot)$ is a loss function. We make the following modeling assumptions:

- A1:** $\ell(\cdot, \cdot)$ is non-negative, symmetric, bounded by a finite positive number L , and satisfies the triangle inequality.
- A2:** The representation function f is invertible when restricted to the intrinsically low-dimensional data manifold.

Assumption A1 can be easily satisfied by any metric or norm truncated by a finite positive number. Concretely, if $d(a, b)$ is a metric, potentially unbounded like Mean Squared Error (MSE), then $loss(a, b) := \min(L, d(a, b))$ satisfies A1. In contrast to our requirements, the loss function in [Redko et al., 2017] is supposed to be convex, symmetric, bounded, obeying the triangle inequality, and satisfying a specific form, while the loss function in [Shen et al., 2018] required to be Lipschitz with respect to the hypothesis due to the use of Wasserstein-1 distance.

Assumption A2 can be explained by the manifold hypothesis that real-world data like images lie in a low-dimensional manifold within a high-dimensional space, which is also the basis of most dimension-reducing mappings such as those based on classical PCA, auto-encoders, etc.. Thus, the dimensional-reducing mapping f can be exactly invertible or nearly so when restricted to an intrinsically low-dimensional data manifold embedded within the high-dimensional ambient space. The same phenomena and its application can also be seen in compressive sampling. For example, it is possible to recover a sparse high dimensional signal which belongs to the union of sub-spaces - a low-dimensional manifold, from a compressed low-dimensional linear mapping. Additionally, note that the success of Generative Adversarial Networks (GAN) [Goodfellow et al., 2014] is also based on transforming a low-dimensional Gaussian to a distribution on an ambient space of high dimension. In practice, invertibility can be approximately achieved if a reconstruction map with a sufficiently

low reconstruction error exists or if the mutual information between the input and its representation is large enough. Indeed, our ablation study in Section 4.1 confirms the usefulness of imposing the invertibility condition in practical algorithms. Finally, although the results in this paper mainly rely on the assumption of invertible maps, we show that this assumption can be relaxed to be nearly invertible with more constraints added, as shown in Appendix B.2.

2.1 Bounds Relating Seen and Unseen Domain Risks

We begin by considering a single seen domain. Lemma 1 below upper bounds the risk $R^{(u)}(h)$ of a hypothesis $h = g \circ f$ in the unseen domain u by three terms: (1) its risk $R^{(s)}(h)$ in a *single* seen domain s , (2) the L^1 distance between the distributions of the *representations* of data from the seen and unseen domain, and (3) a third term $\sigma^{(u,s)}$ that is free of h and is intrinsic to the domains and the loss function. We use the notation $f_{\#}\mu^{(v)}$ to denote the pushforward of distribution of $\mu^{(v)}$, i.e., the distribution of $f(\mathbf{x})$ with $\mathbf{x} \sim \mu^{(v)}$.

Lemma 1. *For any hypothesis $h \in \mathcal{H}$,*

$$R^{(u)}(h) \leq R^{(s)}(h) + L \|f_{\#}\mu^{(u)} - f_{\#}\mu^{(s)}\|_1 + \sigma^{(u,s)}$$

where $\|f_{\#}\mu^{(u)} - f_{\#}\mu^{(s)}\|_1 = \int |f_{\#}\mu^{(u)} - f_{\#}\mu^{(s)}| d\mathbf{x}$ denotes the L^1 distance between $(f_{\#}\mu^{(u)}, f_{\#}\mu^{(s)})$ and

$$\sigma^{(u,s)} := \min \{ \mathbb{E}_{\mathbf{x} \sim \mu^{(u)}} [\ell(h^{(u)}(\mathbf{x}), h^{(s)}(\mathbf{x}))], \mathbb{E}_{\mathbf{x} \sim \mu^{(s)}} [\ell(h^{(u)}(\mathbf{x}), h^{(s)}(\mathbf{x}))] \}.$$

Proof. Please see Appendix B.1. □

The proposed upper bound in Lemma 1 requires f to be invertible. Particularly, the invertibility assumption is employed in the proof of Lemma 1, Eq. (22), Appendix B.1. This condition can be relaxed to be nearly invertible as discussed in Appendix B.2, and implemented by minimizing reconstruction loss or maximizing the mutual information between representation and the input data as discussed in Section 2.2.

In typical applications of DG, training data from multiple seen domains are available, which can be mixed in myriad ways. Lemma 2 below, therefore, extends Lemma 1 to a convex combination of distributions of seen domains.

Lemma 2. *For all convex weights $\lambda^{(1)}, \lambda^{(2)}, \dots, \lambda^{(S)}$ (nonnegative and summing to one) and any hypothesis $h \in \mathcal{H}$,*

$$R^{(u)}(h) \leq \sum_{s=1}^S \lambda^{(s)} R^{(s)}(h) + L \sum_{s=1}^S \lambda^{(s)} \|f_{\#}\mu^{(u)} - f_{\#}\mu^{(s)}\|_1 + \sum_{s=1}^S \lambda^{(s)} \sigma^{(u,s)}.$$

Proof. This follows immediately by taking the convex combination of the bound given by Lemma 1 over the seen domains. □

The upper bound is based on the L^1 distances between the pushforwards of seen and unseen distributions. Estimating L^1 distances accurately from samples is well-known to be hard [Ben-David et al., 2010, Kifer et al., 2004]. To overcome this practical limitation, we upper bound the L^1 distance by the Wasserstein-2 distance under additional regularity assumptions on the pushforwards.

Definition 1. [Polyanskiy and Wu, 2016] A probability distribution on \mathbb{R}^d is called (c_1, c_2) -regular, with $c_1, c_2 \geq 0$, if it is absolutely continuous with respect to the Lebesgue measure with a differentiable density $p(\mathbf{x})$ such that

$$\forall \mathbf{x} \in \mathbb{R}^d, \quad \|\nabla \log_2 p(\mathbf{x})\|_2 \leq c_1 \|\mathbf{x}\|_2 + c_2,$$

where ∇ denotes the gradient and $\|\cdot\|_2$ denotes the standard Euclidean norm.

Lemma 3. If μ and ν are (c_1, c_2) -regular, then

$$\|\mu - \nu\|_1 \leq \sqrt{c_1 \left(\sqrt{\mathbb{E}_{\mathbf{u} \sim \mu} [\|\mathbf{u}\|_2^2]} + \sqrt{\mathbb{E}_{\mathbf{v} \sim \nu} [\|\mathbf{v}\|_2^2]} \right) + 2c_2} \times \sqrt{W_2(\mu, \nu)}$$

where the Wasserstein- p metric [Peyré and Cuturi, 2019, Santambrogio, 2015] $W_p(\mu, \nu)$ is defined as,

$$W_p(\mu, \nu) := \min_{\pi \in \Pi(\mu, \nu)} (\mathbb{E}_{(\mathbf{u}, \mathbf{v}) \sim \pi} [\|\mathbf{u} - \mathbf{v}\|_2^p])^{1/p}$$

where $\Pi(\mu, \nu)$ is the set of joint distributions with marginals μ and ν .

Proof. Please see Appendix B.3. □

One may ask: what conditions guarantee the regularity of the pushforward distributions? Proposition 2 and Proposition 3 in [Polyanskiy and Wu, 2016] show that any distribution ν for which $\mathbb{E}_{\mathbf{v} \sim \nu} \|\mathbf{v}\|_2$ is finite becomes regular when convolved with any regular distribution, including the Gaussian distribution. Since convolution of distributions corresponds to addition of independent random vectors having those distributions, in practice it is always possible to make the pushforwards regular by adding a small amount of independent spherical Gaussian noise in representation space.

Combining Lemma 2, Lemma 3, and Jensen's inequality, we obtain our main result:

Theorem 1. If $f_{\#}\mu^{(s)}$, $s = 1, 2, \dots, S$, and $f_{\#}\mu^{(u)}$ are all (c_1, c_2) -regular, then for all convex weights $\lambda^{(1)}, \lambda^{(2)}, \dots, \lambda^{(S)}$ and any hypothesis $h \in \mathcal{H}$,

$$R^{(u)}(h) \leq \sum_{s=1}^S \lambda^{(s)} R^{(s)}(h) + LC \left[\sum_{s=1}^S \lambda^{(s)} W_2^2(f_{\#}\mu^{(u)}, f_{\#}\mu^{(s)}) \right]^{1/4} + \sum_{s=1}^S \lambda^{(s)} \sigma^{(u,s)} \quad (2)$$

where

$$C = \max_s \sqrt{c_1 \left(\sqrt{\mathbb{E}_{\mathbf{x} \sim \mu^{(u)}} [\|f(\mathbf{x})\|^2]} + \sqrt{\mathbb{E}_{\mathbf{x} \sim \mu^{(s)}} [\|f(\mathbf{x})\|^2]} \right) + 2c_2}.$$

Proof. Please see Appendix B.4. □

It is worth noting that the third term $\sum_{s=1}^S \lambda^{(s)} \sigma^{(u,s)}$ in the upper bound of Theorem 1 is independent of both the representation map f and the labeling function g that contrasts with the previous results in [Ben-David et al., 2007], please see our detailed analysis in Appendix A.1. In addition, one may find the form of the upper bound derived above shares some similarities with Lemma 1 in [Redko et al., 2017] and Theorem 1 in [Shen et al., 2018], for example, all of them introduce Wasserstein distance between domain distributions. But the content is indeed different from previous work based on the following key points.

1. Our upper bound is constructed in the *representation* space, not in the data (ambient) space, which provides a theoretical justification for the risk of unseen domain when decomposing the hypothesis into a representation mapping and a labeling function. This is also consistent with the algorithm implementation in practice.
2. The loss function in [Redko et al., 2017] is assumed to be convex, symmetric, bounded, obeying the triangle inequality, and satisfying a specific form, while in [Shen et al., 2018], it is required to be Lipschitz with respect to the hypothesis due to the use of Wasserstein-1 distance. With fewer constraints posed on the loss function, we only assume it is symmetric, bounded, and satisfies triangle inequality.
3. The bounds in Lemma 1 of [Redko et al., 2017] and Theorem 1 of [Shen et al., 2018] are controlled by the Wasserstein-1 distance, while our upper bound is managed by the square root of the Wasserstein-2 distance. There are regimes where one bound is tighter than the other. Please see the detailed analysis in Appendix A.2.

The bound proposed in Theorem 1 can also be used for the DA problem where one can access the unseen/target domain data and estimate its distribution. However, in the DG setting, due to the unavailability of the unseen data, the second term in (2) is intractable, leading to an intractable upper bound. It is worth noting this intractable bound is widely accepted as a fundamental problem of DG which cannot be overcome without making additional specific assumptions on the unseen domain.

As a step toward developing a practical algorithm based on our new bound, we decompose the second term in (2) into two separate terms, where the second term depends completely on the unseen distribution while the first term can be optimized.

Corollary 1. *Using the notations in Theorem 1, for an arbitrary pushforward distribution $f_{\#}\mu$, we have:*

$$R^{(u)}(h) \leq \sum_{s=1}^S \lambda^{(s)} R^{(s)}(h) + LC \left[\sum_{s=1}^S \lambda^{(s)} W_2^2(f_{\#}\mu, f_{\#}\mu^{(s)}) \right]^{1/4} + LC \left[W_2^2(f_{\#}\mu^{(u)}, f_{\#}\mu) \right]^{1/4} + \sum_{s=1}^S \lambda^{(s)} \sigma^{(u,s)}. \quad (3)$$

Proof. Please see Appendix B.5. □

Motivated by bound in Corollary 1, we seek a suitable $f_{\#}\mu$ to minimize $\sum_{s=1}^S \lambda^{(s)} W_2^2(f_{\#}\mu, f_{\#}\mu^{(s)})$ while ignoring $W_2^2(f_{\#}\mu^{(u)}, f_{\#}\mu)$ since this term is completely intractable. Minimizing $\sum_{s=1}^S \lambda^{(s)} W_2^2(f_{\#}\mu, f_{\#}\mu^{(s)})$

term leads to finding the Wasserstein-2 barycenter of the distributions of seen domains in the representation space. We use uniform weights, i.e., $\lambda^{(s)} = \frac{1}{S}$, since there is, in general, no additional information available to choose the weights of the seen domains. The Wasserstein-2 barycenter of the pushforward distributions of seen domains is defined by:

$$f_{\#}\mu_{barycenter} := \arg \min_{f_{\#}\mu} \sum_{s=1}^S \frac{1}{S} W_2^2(f_{\#}\mu^{(s)}, f_{\#}\mu). \quad (4)$$

We refer the reader to Agueh and Carlier [2011], Cuturi and Doucet [2014] for the definition and properties (existence, uniqueness) of the Wasserstein barycenter.

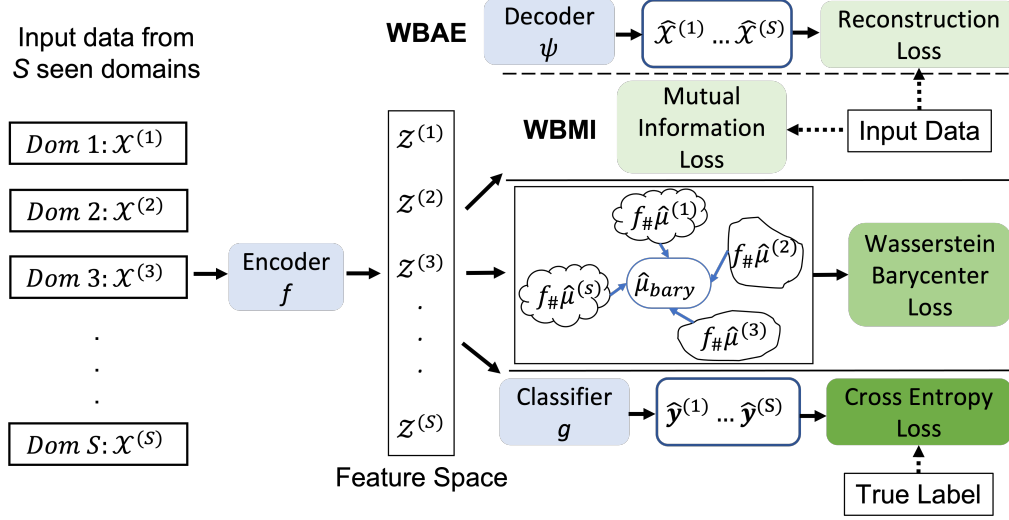


Figure 1: An overview of the proposed algorithms. On the top branch, two sub-branches refer to either choosing WBAE or WBMI.

2.2 Proposed Methods

Since the last term in Theorem 1 and its extension, Corollary 1 is independent of both the representation function f and the labeling function g , and the third term in Corollary 1 is intractable due to its dependence on unseen domain, we thus focus on designing f and g to minimize the first and second terms in Corollary 1

Following previous work [Albuquerque et al., 2019, Ben-David et al., 2007, 2010], we optimize the first term by training f together with g using a standard cross-entropy (CE) loss, such that the empirical classification risk on seen domains is minimized. The classification loss function can be written as:

$$L_c(f, g) = \sum_{s=1}^S \mathbb{E}_{\mathbf{x} \sim \mu^{(s)}} [\text{CE}(h^{(s)}(\mathbf{x}), g(f(\mathbf{x})))] \quad (5)$$

where $\text{CE}(h^{(s)}(\mathbf{x}), g(f(\mathbf{x})))$ denotes the cross entropy (CE) loss between the output of classifier and the ground-truth label of seen domain s .

As previously discussed in Corollary 1, we propose to use the Wasserstein-2 barycenter of representation distributions of seen domains to optimize the second term in Eq. (2) and (3). Specifically, the barycenter loss is defined by:

$$\mathcal{L}_{bary}(f) := \sum_{s=1}^S \frac{1}{S} W_2^2(f_{\#}\mu^{(s)}, f_{\#}\mu_{barycenter}) \quad (6)$$

where $f_{\#}\mu_{barycenter}$, as defined in Eq. (4), denotes the barycenter of pushforward distributions of seen domains.

In contrast to the previous Wasserstein distance-based method in [Zhou et al., 2021a], where pairwise Wasserstein distance loss is employed, we motivate the use of Wasserstein barycenter loss based on our Corollary 1 and demonstrate its ability in enforcing domain-invariance in the ablation study. Further, note that from the definition in (6), computing barycenter loss only requires computing S Wasserstein distances in contrast to $S(S-1)/2$ when using pairwise Wasserstein distances.

Furthermore, to incorporate our assumption that f is manifold restricted invertible, we empirically explore two methods to enforce this constraint, i.e., reconstruction-based method and mutual information-based method.

The first method is inspired by the structure of auto-encoder, which is commonly used for dimension reduction [Wang et al., 2016]. We adopt the encoder-decoder structure and introduce reconstruction loss to approximate the invertibility constraint. Specifically, a decoder $\psi : \mathbb{R}^{d'} \rightarrow \mathbb{R}^d$ is adopted, leading to the following reconstruction loss term:

$$\mathcal{L}_r(f, \psi) := \sum_{s=1}^S \mathbb{E}_{\mathbf{x} \sim \mu^{(s)}} \|\mathbf{x} - \psi(f(\mathbf{x}))\|^2. \quad (7)$$

Another method is motivated by the manifold hypothesis and rate-distortion theory. Particularly, we propose to use mutual information (MI) $I(\mathbf{X}^{(s)}; f(\mathbf{X}^{(s)}))$ [Cover, 1999] between the input of seen domain s and its (noisy) representation as a measure of the invertibility of f . The MI quantifies the dependence between $\mathbf{X}^{(s)}$ and $f(\mathbf{X}^{(s)})$, the larger the mutual information is, the more statistically dependent between the input and its representation. In other words, if f fails to achieve the invertibility, the MI term will be small due to the loss of information after representation mapping. This gives rise to the following mutual information loss term (we inserted a negative sign for minimization):

$$L_i(f) = - \sum_{s=1}^S I(\mathbf{X}^{(s)}; f(\mathbf{X}^{(s)})). \quad (8)$$

From the previous analysis, to enforce the invertibility constraint while balancing the other objectives, we propose two objective functions in Eq. (9) and Eq. (10):

$$\arg \min_{f, g, \psi} \mathcal{L}_c(f, g) + \alpha \mathcal{L}_{bary}(f) + \beta \mathcal{L}_r(f, \psi) \quad (9)$$

and

$$\arg \min_{f, g} \mathcal{L}_c(f, g) + \alpha \mathcal{L}_{bary}(f) + \beta L_i(f) \quad (10)$$

where $\alpha, \beta > 0$ are hyperparameters.

We observe that the terms in our proposed upper bound are incorporated into our objective functions in Eq. (9) and (10). Specifically, the first term in both objective functions aims to determine a good classifier g together with a representation mapping f by minimizing the training error, which corresponds to the first term of the upper bound in Eq. (2). Motivated by the proposed upper bound in Theorem 1 and Corollary 1, the second term in Eq. (9) and (10) acts as a domain alignment tool that aims to minimize the discrepancy between seen domains, contributing to a domain-invariant mapping. Noting that although L_{bary} itself requires solving an optimization problem, we leverage fast computation methods, which is also discussed in Section 3, to directly estimate this loss without invoking the Kantorovich-Rubenstein dual characterization of Wasserstein distances [Santambrogio, 2015]. This avoids solving a min-max type problem that is often plagued by unstable numerical dynamics. Moreover, according to the manifold invertibility assumption required in Theorem 1, we add the third term in Eq. (9) and (10).

3 ALGORITHMS

Based on the loss functions designed above, we propose algorithms to learn domain-invariant but task-sensitive representations. Depending on how the invertibility criteria is dealt with, we design two different algorithms: Wasserstein Barycenter loss with Auto-Encoder (WBAE) and Wasserstein Barycenter loss with Mutual Information (WBMI) which are combined in Algorithm 1. WBAE adopts the auto-encoder structure to maintain the invertibility, while WBMI adds a mutual information term in the loss function for enforcing it. An overview of the proposed methods is shown in Figure 1. Both algorithms involve calculating Wasserstein-2 barycenter and its supporting points. Here we use an off-the-shelf python package [Flamary et al., 2021] that implements a free-support Wasserstein barycenter algorithm described in [Cuturi and Doucet, 2014]. This algorithm is executed in the primal domain and avoids the use of the dual form of Wasserstein distances, which otherwise would turn the problem into an adversarial (min-max) type setting that we want to avoid due to its instability. The barycenter loss is approximated via an average Sinkhorn divergence [Feydy et al., 2019] between the seen domains and the estimated barycenter. Sinkhorn divergence is an unbiased proxy for the Wasserstein distance, which leverages entropic regularization [Cuturi, 2013] for computational efficiency, thereby allowing for integrating automatic differentiation with GPU computation. We adopt the implementation in [Feydy et al., 2019] to our algorithm for a fast gradient computation and denote it as $Sinkhorn_\epsilon$ in Algorithm 1, where ϵ is the entropic regularization term.

For WBAE method, we use an encoder f and a decoder ψ , which are parameterized by θ_e and θ_d , for feature extraction and enforcing the invertibility. Here $\mathcal{X}^{(s)}$ is denoted as a set of samples from domain s with empirical distribution $\hat{\mu}^{(s)}$ with $\mathbf{x}_i^{(s)}$ as one of its element. The corresponding label set of $\mathcal{X}^{(s)}$ is $\mathbf{y}^{(s)}$, where $\mathbf{y}^{(s)} := \{y_i^{(s)}\}$ with $y_i^{(s)}$ is the label for sample $\mathbf{x}_i^{(s)}$. The extracted feature $\mathbf{z}_i^{(s)} = f_{\theta_e}(\mathbf{x}_i^{(s)})$ in set $\mathcal{Z}^{(s)}$ is under the empirical distribution of $f_{\#}\hat{\mu}^{(s)}$. The decoder takes the extracted features as input and outputs the reconstructions as $\psi_{\theta_d}(\mathbf{z}_i^{(s)})$ for domain s . The classifier g , which is parameterized by θ_c is applied to the extracted features for label prediction. As a surrogate of

the decoder ψ_{θ_d} , WBMI maximizes the mutual information between the input data and the extracted feature as an objective to obligate the invertibility. Since mutual information is intractable when the distribution is unknown, we adopt the Mutual Information Gradient Estimation (MIGE) [Wen et al., 2020] framework to estimate the gradient of mutual information between the distribution of the input data and the extracted feature. Moreover, to avoid the mutual information going to infinity, we add a small noise to the extracted feature.

Algorithm 1 Wasserstein Barycenter Loss with Auto-Encoder/ Mutual Information (WBAE/WBMI)

Input: Data from S seen domains, batch size m , learning rate η , parameters $\alpha, \beta, \epsilon, \delta$. **Output:** Encoder f_{θ_e} , decoder ψ_{θ_d} , classifier g_{θ_c}

```

1: while training is not end do
2:   Randomly choose  $m$  samples from each domain, denoted as  $\mathcal{X}^{(s)} := \{\mathbf{x}_i^{(s)}\}_{i=1}^m \sim \hat{\mu}^{(s)}$  and
      $\mathbf{y}^{(s)} := \{y_i^{(s)}\}_{i=1}^m$ 
3:   for  $s = 1 : S$  and  $i = 1 : m$  do
4:      $\mathbf{z}_i^{(s)} \leftarrow f_{\theta_e}(\mathbf{x}_i^{(s)})$  with set  $\mathcal{Z}^{(s)} \sim f_{\#}\hat{\mu}^{(s)}$ 
5:     if WBMI then
6:        $\mathcal{Z}_{noise}^{(s)} \leftarrow \mathcal{Z}^{(s)} + \delta\mathcal{N}(0, 1)$ 
7:     end if
8:   end for
9:   Calculate the Wasserstein barycenter  $\hat{\mu}_{bary}$  of  $\{f_{\#}\hat{\mu}^{(s)}\}_{s=1}^S$  and its supporting points with  $f_{\theta_e}$ 
     detached from automatic backpropagation
10:   $\mathcal{L}_{wb} \leftarrow \frac{1}{S} \sum_{s=1}^S Sinkhorn_{\epsilon}(\hat{\mu}_{bary}, f_{\#}\hat{\mu}^{(s)})$ 
11:   $\mathcal{L}_c \leftarrow -\frac{1}{m} \sum_{s=1}^S \sum_{i=1}^m y_i^s \log p(g_{\theta_c}(f_{\theta_e}(\mathbf{x}_i^{(s)})))$ 
12:  if WBAE then
13:     $\mathcal{L}_r \leftarrow \frac{1}{m} \sum_{s=1}^S \sum_{i=1}^m \|\mathbf{x}_i^{(s)} - \psi_{\theta_d}(\mathbf{z}_i^{(s)})\|_2^2$ 
14:     $\mathcal{L} \leftarrow \mathcal{L}_c + \alpha\mathcal{L}_{wb} + \beta\mathcal{L}_r$ 
15:     $\theta_c \leftarrow \theta_c - \eta\nabla_{\theta_c}\mathcal{L}_c, \quad \theta_d \leftarrow \theta_d - \eta\nabla_{\theta_d}\mathcal{L}_r$ 
16:     $\theta_e \leftarrow \theta_e - \eta\nabla_{\theta_e}\mathcal{L}$ 
17:  end if
18:  if WBMI then
19:    Estimate the gradient of mutual information between the empirical distribution of  $\{\mathcal{X}^{(s)}\}_{s=1}^S$ 
       and  $\{\mathcal{Z}_{noise}^{(s)}\}_{s=1}^S$  via MIGE, denoted as  $\nabla_{\theta_e}\mathcal{L}_i$ 
20:     $\theta_c \leftarrow \theta_c - \eta\nabla_{\theta_c}\mathcal{L}_c$ 
21:     $\theta_e \leftarrow \theta_e - \eta(\alpha\nabla_{\theta_e}\mathcal{L}_{wb} + \beta\nabla_{\theta_e}\mathcal{L}_i)$ 
22:  end if
23: end while

```

4 EXPERIMENTS AND RESULTS

The proposed methods were evaluated on two widely used DG datasets: VLCS Fang et al. [2013] and Office-Home [Venkateswara et al., 2017] and compared with various *theory-guided* DG algorithms. We implemented the proposed methods following Gulrajani’s work Gulrajani and Lopez-Paz [2021] and their DomainBed suite to facilitate the comparison with the results reported therein.

Datasets: The **VLCS** dataset Fang et al. [2013] consists of images from 4 different domains: VOC2007 (V), LabelMe (L), Caltech (C), PASCAL (S). A total of 5 classes are shared by all domains. The **Office-Home** dataset [Venkateswara et al., 2017] is a larger and more challenging dataset with 15,500 images from 4 different domains: Artistic images (A), Clipart (C), Product (P), and Real-World (R). Each domain has 65 object categories.

Model Structure: We used an ImageNet pre-trained ResNet-50 model with the final (softmax) layer replaced by three fully connected (FC) layers ($2048 \rightarrow 1024 \rightarrow 512 \rightarrow 200$) as the feature extractor. Here we slightly deviated from the implementation in Gulrajani and Lopez-Paz [2021] by further decreasing the dimension of the extracted feature from 2048 to 200 due to the high cost of estimating the gradient of the mutual information for high dimensional data. The decoder comprises two FC layers ($200 \rightarrow 512 \rightarrow 2048$) followed by three ConvTranspose2d layers. The detailed structure of the decoder is described in Table 4 within Appendix C. The classifier is a one-linear-layer model with the output dimension the same as the number of classes.

Hyper-parameters: Due to the limitation of computational resources, we set all hyper-parameters (e.g., learning rate, batch size, dropout, etc.) to the default values shown in Table 6 of Gulrajani and Lopez-Paz [2021] and use the Adam optimizer Kingma and Ba [2015] for optimization. The values of δ for Gaussian noise and ϵ for the Sinkhorn loss (line 6 and 10, Algorithm 1) are also empirically set to 0.1 and 0.5, respectively, without tuning. We only tune two hyper-parameters, namely the weights α and β . We perform a grid search over the set $\{0.0001, 0.0005\}$ for α and $\{0.0001, 0.0005, 0.001, 0.005\}$ for β . A complete list of all hyper-parameters is shown in Table 5 in Appendix C.

Model Selection: We adopted the commonly used training-domain validation strategy in Gulrajani and Lopez-Paz [2021], Krueger et al. [2021] for hyper-parameter tuning and model selection. Specifically, we split the data from each domain into training and validation sets in the proportion 80% and 20%, respectively. During training, we aggregated together the training/validation samples from each seen domain to form the overall training/validation set and selected the model with the highest validation accuracy for testing.

Model Evaluation: We followed the commonly used leave-one-domain-out evaluation strategy Gulrajani and Lopez-Paz [2021], Dou et al. [2019]: one domain is left out as the unseen test domain and the remaining domains are treated as the seen domains. Following Gulrajani and Lopez-Paz [2021], hyper-parameters were re-optimized for every new test unseen domain.

Comparison Methods: In this paper, we compare the empirical performance of our proposed methods against the state-of-the-art DG methods reported in Gulrajani and Lopez-Paz [2021]. We can divide the algorithms tested in Gulrajani and Lopez-Paz [2021] into two categories: (a) heuristic algorithms unsupported by theoretical analysis for the DG problem, and (b) theory-guided algorithms.

For a fair comparison, we mainly focus on the methods in group (b) where algorithms are supported by a theoretical analysis of the DG problem. These are:

- Empirical Risk Minimization (**ERM**) Vapnik [1999] which aims to minimize the cumulative training error across all seen domains.
- Domain-Adversarial Neural Networks (**DANN**) Ganin et al. [2016] which is motivated by the theoretical results from Ben-David et al. [2007]. In particular, to minimize the upper bound of the risk in the unseen domain, **DANN** adopts an adversarial network to enforce that features from different domains are indistinguishable.
- Class-conditional DANN (**C-DANN**) Li et al. [2018b] is a variant of **DANN** that aims to match not only the feature distributions between domains but also match the conditional distributions of the label given the data across domains.
- Invariant Risk Minimization (**IRM**) Arjovsky et al. [2019] aims to learn features such that the optimal classifiers applied to these features are matched across domains.
- Risk Extrapolation (**VREx**) Krueger et al. [2021] is constructed on the assumption from Arjovsky et al. [2019] that there exists an optimal linear classifier across all domains. While **IRM** specifically seeks the invariant classifier, **VREx** aims to identify the form of the distribution shift, leading to the robustness for a wider variety of distributional shifts.
- Marginal Transfer Learning (**MTL**) Blanchard et al. [2011, 2021] is proposed based on an upper bound for the generalization error under the setting of an Agnostic Generative Model. Specifically, **MTL** estimates the mean embedding per domain and uses it as a second argument for optimizing the classifier.
- **CORAL** Sun and Saenko [2016] is based on the idea of matching the mean and covariance of feature distributions from different domains.

Here, **ERM** acts as the baseline theory-guided model and **DANN**, **C-DANN**, **IRM**, **VREx**, **MTL** are five state-of-the-art theory-guided algorithms. Besides these six methods, for a complete comparison we also include **CORAL** Sun and Saenko [2016], a heuristic algorithm that achieves the best performance on the evaluated datasets Gulrajani and Lopez-Paz [2021].

We use Nvidia-tesla p100 16 GB GPU for computation. A single round of training for one task took about forty minutes for WBAE and one hour for WBMI. The whole experiment is repeated three times with different random seeds and the average accuracy and standard deviation are reported in Tables 1 and 2. Results of all comparison methods are taken from Gulrajani and Lopez-Paz [2021].

Results: Results for VLCS dataset are shown in Table 1. Both WBAE and WBMI achieve comparable results with the state-of-the-art methods. In particular, the WBAE method achieves the highest accuracy in two of four domains and has a modest improvement over all theory-guided and the best-performing heuristic DG methods. An obvious improvement can be seen in Table 2 when

examining the proposed methods on Office-Home, a larger and more challenging dataset. Both WBAE and WBMI outperform the theory-guided comparison methods by at least 2.3% points on average and at least 3.4%, 1.8%, 1.3% and 1.6% points on each task. A similar or slightly better performance can be observed when comparing WBAE and WBMI with the best-performing heuristic method CORAL.

Table 1: Performance on VLCS dataset measured by accuracy (%). C, L, S, V are left-out unseen domain.

Algorithm	C	L	S	V	Avg
ERM	97.7 \pm 0.4	64.3 \pm 0.9	73.4 \pm 0.5	74.6 \pm 1.3	77.5 \pm 0.4
IRM	98.6 \pm 0.1	64.9 \pm 0.9	73.4 \pm 0.6	77.3 \pm 0.9	78.5 \pm 0.5
DANN	99.0 \pm 0.3	65.1 \pm 1.4	73.1 \pm 0.3	77.2 \pm 0.6	78.6 \pm 0.4
CDANN	97.1 \pm 0.3	65.1 \pm 1.2	70.7 \pm 0.8	77.1 \pm 1.5	77.5 \pm 0.1
MTL	97.8 \pm 0.4	64.3 \pm 0.3	71.5 \pm 0.7	75.3 \pm 1.7	77.2 \pm 0.4
VREx	98.4 \pm 0.3	64.4 \pm 1.4	74.1 \pm 0.4	76.2 \pm 1.3	78.3 \pm 0.2
CORAL	98.3 \pm 0.1	66.1 \pm 1.2	73.4 \pm 0.3	77.5 \pm 1.2	78.8 \pm 0.6
WBAE	98.0 \pm 0.5	66.8 \pm 1.0	75.0 \pm 2.1	76.0 \pm 0.9	79.0 \pm 0.5
WBMI	97.4 \pm 0.7	64.7 \pm 0.9	71.6 \pm 1.6	75.1 \pm 1.6	77.2 \pm 0.5

4.1 Ablation Study

To study the impact of different components of the total loss function, we conducted an ablation study for WBAE and WBMI on both datasets. In particular, we consider the following variants of our method: (1) WBAE- L_{wb} : WBAE without Wasserstein barycenter loss; (2) WBAE- L_r /WBMI- L_i : WBAE without reconstruction loss. Since this variant can also be viewed as WBMI method without mutual information loss, we also denote it as WBMI- L_i ; (3) WBMI- L_{wb} : WBMI method without Wasserstein barycenter loss; (4) WBAE: original WBAE method with all the loss components; (5) WBMI: original WBMI method with all the loss components. We re-ran all the experiments three times using the same model architectures, hyper-parameter tuning and validation processes.

From Table 3, we find that removing L_r from WBAE model leads to a decrease in the accuracy of around 1.8% points for VLCS dataset and 0.1% points for Office-Home dataset. The performance deterioration can be more clearly observed when omitting L_{wb} for WBAE model, leading to a drop of around 1.9% points for the VLCS dataset and 4.6% points for the Office-Home dataset. A similar trend can be found for the WBMI model, especially for the Office-Home dataset, where the accuracy drops by 0.3% points when removing the mutual information loss L_i and 5.3% points with the Wasserstein barycenter loss L_{wb} removed. Note that we do not include ERM for comparison in the ablation study since extensive hyper-parameter tuning has already been conducted and reported for the ERM method in Gulrajani and Lopez-Paz [2021].

This ablation study demonstrates the importance of the Wasserstein barycenter loss and also shows the auxiliary role of the invertibility of the representation mapping. This is reflected in the obvious

Table 2: Performance on Office-Home dataset measured by accuracy (%). A, C, P, R are left-out unseen domain.

Algorithm	A	C	P	R	Avg
ERM	61.3 \pm 0.7	52.4 \pm 0.3	75.8 \pm 0.1	76.6 \pm 0.3	66.5 \pm 0.3
IRM	58.9 \pm 2.3	52.2 \pm 1.6	72.1 \pm 2.9	74.0 \pm 2.5	64.3 \pm 2.2
DANN	59.9 \pm 1.3	53.0 \pm 0.3	73.6 \pm 0.7	76.9 \pm 0.5	65.9 \pm 0.6
CDANN	61.5 \pm 1.4	50.4 \pm 2.4	74.4 \pm 0.9	76.6 \pm 0.8	65.8 \pm 1.3
MTL	61.5 \pm 0.7	52.4 \pm 0.6	74.9 \pm 0.4	76.8 \pm 0.4	66.4 \pm 0.5
VREx	60.7 \pm 0.9	53.0 \pm 0.9	75.3 \pm 0.1	76.6 \pm 0.5	66.4 \pm 0.6
CORAL	65.3 \pm 0.4	54.4 \pm 0.5	76.5 \pm 0.1	78.4 \pm 0.5	68.7 \pm 0.3
WBAE	64.9 \pm 0.8	54.9 \pm 0.8	76.6 \pm 0.5	78.5 \pm 0.8	68.7 \pm 0.2
WBMI	65.2 \pm 0.8	54.8 \pm 0.9	76.9 \pm 0.3	78.5 \pm 0.3	68.9 \pm 0.3

Table 3: Ablation study for WBAE and WBMI on VLCS and Office-Home datasets.

Dataset	WBAE- L_{wb}	WBAE- L_r WBMI- L_i	WBMI- L_{wb}	WBAE	WBMI
VLCS	77.1 \pm 0.7	77.2 \pm 0.6	77.0 \pm 0.1	79.0 \pm 0.5	77.2 \pm 0.5
Office-Home	64.1 \pm 0.2	68.6 \pm 0.6	63.6 \pm 0.1	68.7 \pm 0.2	68.9 \pm 0.3

performance improvement when adding Wasserstein barycenter loss L_{wb} for both methods and a less significant improvement when introducing L_r/L_i . On the other hand, the results indicate that the estimation of the gradient for mutual information may not be accurate and stable in higher dimensions, which is one limitation of the proposed WBMI method.

5 CONCLUSION AND FUTURE WORK

We revisited the theory and methods for DG and provided a new upper bound for the risk in the unseen domain. Our analysis could be potentially tightened towards understanding minimal regularity conditions on the distribution and the loss functions that can yield better bounds or a family of bounds adapted to different situations. In terms of algorithms and numerical implementation, we note that although our theory-guided methods have better accuracy compared to state-of-the-art approaches, they could be computationally expensive. This high cost is primarily incurred in estimating the Wasserstein-2 barycenter and the gradient of mutual information for high-dimensional data. To alleviate these problems, we could potentially leverage the recently proposed large-scale-barycenter and mapping estimators [Fan et al., 2020] to enable a larger amount of samples for barycenter calculation and also make use of some recent advances in mutual information estimation Spring and Shrivastava [2021].

References

- M. Agueh and G. Carlier. Barycenters in the Wasserstein space. *SIAM Journal on Mathematical Analysis*, 43(2):904–924, 2011.
- I. Albuquerque, J. Monteiro, M. Darvishi, T. H. Falk, and I. Mitliagkas. Generalizing to unseen domains via distribution matching. *arXiv preprint arXiv:1911.00804*, 2019.
- M. Arjovsky, L. Bottou, I. Gulrajani, and D. Lopez-Paz. Invariant risk minimization. *arXiv preprint arXiv:1907.02893*, 2019.
- S. Ben-David, J. Blitzer, K. Crammer, F. Pereira, et al. Analysis of representations for domain adaptation. *Advances in neural information processing systems*, 19:137, 2007.
- S. Ben-David, J. Blitzer, K. Crammer, A. Kulesza, F. Pereira, and J. W. Vaughan. A theory of learning from different domains. *Machine learning*, 79(1):151–175, 2010.
- D. Berend, P. Harremoës, and A. Kontorovich. Minimum kl-divergence on complements of l_1 balls. *IEEE Transactions on Information Theory*, 60(6):3172–3177, 2014. doi: 10.1109/TIT.2014.2301446.
- G. Blanchard, G. Lee, and C. Scott. Generalizing from several related classification tasks to a new unlabeled sample. *Advances in neural information processing systems*, 24:2178–2186, 2011.
- G. Blanchard, A. A. Deshmukh, U. Dogan, G. Lee, and C. Scott. Domain generalization by marginal transfer learning. *Journal of machine learning research*, 2021.
- T. M. Cover. *Elements of information theory*. John Wiley & Sons, 1999.
- I. Csiszár and J. Körner. *Information theory: coding theorems for discrete memoryless systems*. Cambridge University Press, 2011.
- Y. Cui, Y. Xu, and D. Wu. EEG-based driver drowsiness estimation using feature weighted episodic training. *IEEE transactions on neural systems and rehabilitation engineering*, 27(11):2263–2273, 2019.
- M. Cuturi. Sinkhorn distances: Lightspeed computation of optimal transport. *Advances in neural information processing systems*, 26:2292–2300, 2013.
- M. Cuturi and A. Doucet. Fast computation of wasserstein barycenters. In *International conference on machine learning*, pages 685–693. PMLR, 2014.
- Q. Dou, D. C. Castro, K. Kamnitsas, and B. Glocker. Domain generalization via model-agnostic learning of semantic features. *arXiv preprint arXiv:1910.13580*, 2019.
- J. Fan, A. Taghvaei, and Y. Chen. Scalable computations of wasserstein barycenter via input convex neural networks. *arXiv preprint arXiv:2007.04462*, 2020.

- C. Fang, Y. Xu, and D. N. Rockmore. Unbiased metric learning: On the utilization of multiple datasets and web images for softening bias. In *Proceedings of the IEEE International Conference on Computer Vision*, pages 1657–1664, 2013.
- J. Feydy, T. Séjourné, F.-X. Vialard, S.-i. Amari, A. Trounev, and G. Peyré. Interpolating between optimal transport and MMD using sinkhorn divergences. In *The 22nd International Conference on Artificial Intelligence and Statistics*, pages 2681–2690, 2019.
- R. Flamary, N. Courty, A. Gramfort, M. Z. Alaya, A. Boisbunon, S. Chambon, L. Chapel, A. Corenflos, K. Fatras, N. Fournier, L. Gautheron, N. T. Gayraud, H. Janati, A. Rakotomamonjy, I. Redko, A. Rolet, A. Schutz, V. Seguy, D. J. Sutherland, R. Tavenard, A. Tong, and T. Vayer. Pot: Python optimal transport. *Journal of Machine Learning Research*, 22(78):1–8, 2021. URL <http://jmlr.org/papers/v22/20-451.html>.
- Y. Ganin, E. Ustinova, H. Ajakan, P. Germain, H. Larochelle, F. Laviolette, M. Marchand, and V. Lempitsky. Domain-adversarial training of neural networks. *The journal of machine learning research*, 17(1):2096–2030, 2016.
- M. Ghifary, W. B. Kleijn, M. Zhang, and D. Balduzzi. Domain generalization for object recognition with multi-task autoencoders. In *Proceedings of the IEEE international conference on computer vision*, pages 2551–2559, 2015.
- I. Goodfellow, J. Pouget-Abadie, M. Mirza, B. Xu, D. Warde-Farley, S. Ozair, A. Courville, and Y. Bengio. Generative adversarial nets. *Advances in neural information processing systems*, 27, 2014.
- I. Gulrajani and D. Lopez-Paz. In search of lost domain generalization. In *International Conference on Learning Representations*, 2021. URL <https://openreview.net/forum?id=lQdXeXDoWtI>.
- D. Kifer, S. Ben-David, and J. Gehrke. Detecting change in data streams. In *VLDB*, volume 4, pages 180–191. Toronto, Canada, 2004.
- D. P. Kingma and J. Ba. Adam: A method for stochastic optimization. In Y. Bengio and Y. LeCun, editors, *3rd International Conference on Learning Representations, ICLR 2015, San Diego, CA, USA, May 7-9, 2015, Conference Track Proceedings*, 2015. URL <http://arxiv.org/abs/1412.6980>.
- D. Krueger, E. Caballero, J.-H. Jacobsen, A. Zhang, J. Binas, D. Zhang, R. Le Priol, and A. Courville. Out-of-distribution generalization via risk extrapolation (rex). In *International Conference on Machine Learning*, pages 5815–5826. PMLR, 2021.
- N. Lei, D. An, Y. Guo, K. Su, S. Liu, Z. Luo, S.-T. Yau, and X. Gu. A geometric understanding of deep learning. *Engineering*, 6(3):361–374, 2020. ISSN 2095-8099. doi: <https://doi.org/10.1016/j.eng.2019.09.010>. URL <https://www.sciencedirect.com/science/article/pii/S2095809919302279>.
- H. Li, S. J. Pan, S. Wang, and A. C. Kot. Domain generalization with adversarial feature learning. In *Proceedings of the IEEE Conference on Computer Vision and Pattern Recognition*, pages 5400–5409, 2018a.

- Y. Li, X. Tian, M. Gong, Y. Liu, T. Liu, K. Zhang, and D. Tao. Deep domain generalization via conditional invariant adversarial networks. In *Proceedings of the European Conference on Computer Vision (ECCV)*, pages 624–639, 2018b.
- B. Lyu, T. Pham, G. Blaney, Z. Haga, A. Sassaroli, S. Fantini, and S. Aeron. Domain adaptation for robust workload level alignment between sessions and subjects using fNIRS. *Journal of Biomedical Optics*, 26(2):1 – 21, 2021. doi: 10.1117/1.JBO.26.2.022908. URL <https://doi.org/10.1117/1.JBO.26.2.022908>.
- H. Nam, H. Lee, J. Park, W. Yoon, and D. Yoo. Reducing domain gap by reducing style bias. In *Proceedings of the IEEE/CVF Conference on Computer Vision and Pattern Recognition*, pages 8690–8699, 2021.
- G. Peyré and M. Cuturi. Computational optimal transport. *Foundations and Trends in Machine Learning*, 11 (5-6):355–602, 2019.
- Y. Polyanskiy and Y. Wu. Wasserstein continuity of entropy and outer bounds for interference channels. *IEEE Transactions on Information Theory*, 62(7):3992–4002, 2016.
- I. Redko, A. Habrard, and M. Sebban. Theoretical analysis of domain adaptation with optimal transport. In *Joint European Conference on Machine Learning and Knowledge Discovery in Databases*, pages 737–753. Springer, 2017.
- F. Santambrogio. *Optimal Transport for Applied Mathematicians: Calculus of Variations, PDEs and Modeling*. Springer, 2015.
- J. Shen, Y. Qu, W. Zhang, and Y. Yu. Wasserstein distance guided representation learning for domain adaptation. In *Thirty-Second AAAI Conference on Artificial Intelligence*, 2018.
- R. Spring and A. Shrivastava. Mutual information estimation using LSH sampling. In *Proceedings of the Twenty-Ninth International Conference on International Joint Conferences on Artificial Intelligence*, pages 2807–2815, 2021.
- B. Sun and K. Saenko. Deep coral: Correlation alignment for deep domain adaptation. In *European conference on computer vision*, pages 443–450. Springer, 2016.
- V. N. Vapnik. An overview of statistical learning theory. *IEEE transactions on neural networks*, 10(5): 988–999, 1999.
- H. Venkateswara, J. Eusebio, S. Chakraborty, and S. Panchanathan. Deep hashing network for unsupervised domain adaptation. In *Proceedings of the IEEE conference on computer vision and pattern recognition*, pages 5018–5027, 2017.
- J. Wang, C. Lan, C. Liu, Y. Ouyang, and T. Qin. Generalizing to unseen domains: A survey on domain generalization. *arXiv e-prints*, pages arXiv–2103, 2021.

- Y. Wang, H. Yao, and S. Zhao. Auto-encoder based dimensionality reduction. *Neurocomputing*, 184: 232–242, 2016.
- L. Wen, Y. Zhou, L. He, M. Zhou, and Z. Xu. Mutual information gradient estimation for representation learning. In *International Conference on Learning Representations*, 2020. URL <https://openreview.net/forum?id=ByxaUgrFvH>.
- H. Zhao, R. T. Des Combes, K. Zhang, and G. Gordon. On learning invariant representations for domain adaptation. In *International Conference on Machine Learning*, pages 7523–7532. PMLR, 2019.
- F. Zhou, Z. Jiang, C. Shui, B. Wang, and B. Chaib-draa. Domain generalization via optimal transport with metric similarity learning. *Neurocomputing*, 456:469–480, 2021a. ISSN 0925-2312. doi: <https://doi.org/10.1016/j.neucom.2020.09.091>. URL <https://www.sciencedirect.com/science/article/pii/S0925231221002009>.
- K. Zhou, Z. Liu, Y. Qiao, T. Xiang, and C. C. Loy. Domain generalization: A survey. *arXiv preprint arXiv:2103.02503*, 2021b.

A COMPARISON OF UPPER BOUNDS

A.1 Shortcomings of Previously Proposed Upper Bounds

First, recall that a *domain* v is a triple $(\mu^{(v)}, f^{(v)}, g^{(v)})$ consisting of a distribution $\mu^{(v)}$ on the inputs $\mathbf{x} \in \mathbb{R}^d$, a representation function that maps an input \mathbf{x} from input space to its representation \mathbf{z} in the representation space $f^{(v)} : \mathbb{R}^d \rightarrow \mathbb{R}^{d'}$, and a stochastic labeling function $g^{(v)} : \mathbb{R}^{d'} \rightarrow \mathcal{Y}$ maps the representation space $\mathbb{R}^{d'}$ to a label space \mathcal{Y} .

We denote the unseen domain by $(\mu^{(u)}, f^{(u)}, g^{(u)})$ and the seen domain by $(\mu^{(s)}, f^{(s)}, g^{(s)})$. Let $\mathcal{F} = \{f | f : \mathbb{R}^d \rightarrow \mathbb{R}^{d'}\}$ be a set of *representation functions*, $\mathcal{G} = \{g | g : \mathbb{R}^{d'} \rightarrow \mathcal{Y}\}$ a set of stochastic *labeling functions*. Here, the label space \mathcal{Y} is considered as binary. A *hypothesis* $h : \mathbb{R}^d \rightarrow \mathcal{Y}$ is obtained by composing each $g \in \mathcal{G}$ with each $f \in \mathcal{F}$, i.e., $h = g \circ f$. Next, we rewrite Theorem 1 in [Ben-David et al., 2007] using our notations.

Theorem 2. [Ben-David et al., 2007] *Let f be a fixed representation function from input space to representation space and \mathcal{G} be a hypothesis space of VC-dimension k . If a random labeled sample of size m is generated by applying f to i.i.d. samples from the seen domain, then with probability at least $1 - \delta$, for every $g \in \mathcal{G}$:*

$$R^{(u)}(g) \leq R^{(s)}(g) + d_{\mathcal{H}}(f_{\#}\mu^{(u)}, f_{\#}\mu^{(s)}) + \lambda \quad (11)$$

$$\leq \hat{R}^{(s)}(g) + \sqrt{\frac{4}{m} \left(k \log \frac{2em}{k} + \log \frac{4}{\delta} \right)} + d_{\mathcal{H}}(f_{\#}\mu^{(u)}, f_{\#}\mu^{(s)}) + \lambda \quad (12)$$

where e is the base of the natural logarithm, $d_{\mathcal{H}}$ is \mathcal{H} -divergence (please see Definition 1 in [Ben-David et al., 2010], Definition 2.1 in [Zhao et al., 2019] or Definition 1 in [Kifer et al., 2004]), $R^{(u)}(g) = \mathbb{E}_{\mathbf{z} \sim f_{\#}\mu^{(u)}} |g(\mathbf{z}) - g^{(u)}(\mathbf{z})|$ denotes the risk in the unseen domain, $R^{(s)}(g) = \mathbb{E}_{\mathbf{z} \sim f_{\#}\mu^{(s)}} |g(\mathbf{z}) - g^{(s)}(\mathbf{z})|$ and $\hat{R}^{(s)}(g)$ denote the risk in the seen domain and its empirical estimation, respectively, and:

$$\lambda = \inf_{g \in \mathcal{G}} (R^{(s)}(g) + R^{(u)}(g)) \quad (13)$$

is the combined risk.

Although the bound in Theorem 1 of [Ben-David et al., 2007] was originally constructed for the domain adaptation problem, it has significantly influenced past and recent work in domain generalization as discussed earlier in Section 1. To highlight the differences between our work and previous theoretical bounds (the bound in Theorem 1 of [Ben-David et al., 2007] and Theorem 4.1 of [Zhao et al., 2019]), we provide a detailed comparison below:

- First, Ben-David et al. [2007] define the risk induced by labeling function g from the representation space to the label space based on the disagreement between g and the optimal labeling function $g^{(u)}$:

$$R^{(u)}(g) = \mathbb{E}_{\mathbf{z} \sim f_{\#}\mu^{(u)}} |g(\mathbf{z}) - g^{(u)}(\mathbf{z})|. \quad (14)$$

On the other hand, we define the risk induced by using a hypothesis h from input space to label space by the disagreement between h and the optimal hypothesis $h^{(u)}$ via a general loss function

$\ell(\cdot, \cdot)$:

$$R^{(u)}(h) = \mathbb{E}_{\mathbf{x} \sim \mu^{(u)}} [\ell(h(\mathbf{x}), h^{(u)}(\mathbf{x}))]. \quad (15)$$

Since the empirical risk measures the probability of misclassification of a hypothesis that maps from the input space to the label space, minimizing $R^{(u)}(g)$ does not guarantee minimizing the empirical risk. Particularly, if the representation function f is invertible i.e., there is a one-to-one mapping between \mathbf{x} and \mathbf{z} , and the loss function $\ell(a, b) = |a - b|$, then it is possible to verify that $R^{(u)}(g) = R^{(u)}(h)$. In general, the representation map might not be invertible. For example, let us consider a representation function f that maps $f(\mathbf{x}_1) = f(\mathbf{x}_2) = \mathbf{z}$, $\mathbf{x}_1 \neq \mathbf{x}_2$, with corresponding labels given by $y_1 = 0$ and $y_2 = 1$. In this case, the risk defined in (14) will introduce a larger error than the risk introduced in (15) since $g(\mathbf{z})$ cannot be mapped to both "0" and "1". That said, the risk defined in (15) is more precise to describe the empirical risk. In addition, the risk defined in (14) is only a special case of (15) when the representation map f is invertible and the loss function satisfies $\ell(a, b) = |a - b|$.

- Second, for a given hypothesis space, the ideal joint hypothesis g^* is defined as the hypothesis which globally minimizes the combined error from seen and unseen domains [Ben-David et al., 2007, 2010]:

$$g^* = \arg \min_{g \in \mathcal{G}} (R^{(s)}(g) + R^{(u)}(g)).$$

In other words, this hypothesis should work well in both domains. Next, the error induced by using this ideal joint hypothesis is called *combined risk*:

$$\lambda = \inf_{g \in \mathcal{G}} (R^{(s)}(g) + R^{(u)}(g)) = (R^{(s)}(g^*) + R^{(u)}(g^*)).$$

Note that the labeling function is a mapping from the representation space to the label space, therefore the ideal labeling function g^* depends implicitly on the representation function f , hence, λ must depend on f . Simply ignoring this fact and treating λ as a constant may loosen the upper bound. In contrast, our goal is to construct an upper bound with the *combined risk* term $\sigma^{(u,s)}$ independent of both the representation function and the labeling function, which can be seen from Lemma 1 and Theorem 1.

Finally, it is worth comparing our upper bound with the bound in Theorem 4.1 of [Zhao et al., 2019] which also has the *combined risk* term free of the choice of the hypothesis class. However, note that the result in Theorem 4.1 of [Zhao et al., 2019] does not consider any representation function f , i.e., their labeling function directly maps from the input space to the label space, while our hypothesis is composed of a representation function from input space to representation space followed by a labeling function from representation space to label space. Since it is possible to pick a representation function f that maps any input to itself, i.e., $f(\mathbf{x}) = \mathbf{x}$ which leads to $h = g \circ f = g$, the bound in [Zhao et al., 2019] can be viewed as a special case of our proposed upper bound in Lemma 1.

A.2 Comparison with Upper Bounds in [Redko et al., 2017] and [Shen et al., 2018]

The form of the upper bound derived in Theorem 1 shares some similarities with Lemma 1 in [Redko et al., 2017] and Theorem 1 in [Shen et al., 2018], for example, all of them introduce Wasserstein distance between domain distributions. However, they differ in the following key aspects.

1. Our upper bound is constructed in the *representation* space, not in the data (ambient) space, which provides a theoretical justification for the risk of unseen domain when decomposing the hypothesis into a representation mapping and a labeling function. This is also consistent with the algorithmic implementation in practice.
2. The loss function in [Redko et al., 2017] is assumed to be convex, symmetric, bounded, obeying the triangle inequality, and satisfying a specific form, while in [Shen et al., 2018], it is required to be Lipschitz with respect to the hypothesis due to the use of Wasserstein-1 distance. With less constraints imposed on the loss function, we only assume it is symmetric, bounded, and satisfies the triangle inequality.
3. The bounds in Lemma 1 of [Redko et al., 2017] and Theorem 1 of [Shen et al., 2018] are controlled by the Wasserstein-1 distance while our upper bound is managed by the square-root of the Wasserstein-2 distance. There are regimes where one bound is tighter than the other. First, it is well-known that $W_1(\mu, \nu) \leq W_2(\mu, \nu)$, if $W_2(\mu, \nu) \leq 1$, then $W_1(\mu, \nu) \leq \sqrt{W_2(\mu, \nu)}$. However, based on Jensen's inequality, it is possible to show that $\sqrt{W_2(\mu, \nu)} \leq [Diam(f(\mathbf{X}))W_1(\mu, \nu)]^{1/4}$ where $Diam(f(\mathbf{X}))$ denotes the largest distance between two points in the representation space $\mathbb{R}^{d'}$ generated by input \mathbf{X} via mapping f . To guarantee $\sqrt{W_2(\mu, \nu)} \leq W_1(\mu, \nu)$, a sufficient condition is $[Diam(f(\mathbf{X}))W_1(\mu, \nu)]^{1/4} \leq W_1(\mu, \nu)$ which is equivalent to $Diam(f(\mathbf{X})) \leq W_1(\mu, \nu)^3$. In fact, for a given $Diam(f(\mathbf{X}))$, the larger the value of $W_1(\mu, \nu)$, the higher the chance that this sufficient condition will hold.

B PROOFS

B.1 Proof of Lemma 1

First, we want to note that our approach for constructing the upper bound in Lemma 1 is motivated by the proof of Theorem 1 in [Ben-David et al., 2010]. Next, to make the dependence on the hypothesis, input distribution, and the true representation and labeling functions transparent, we use inner product notation $\langle \cdot, \cdot \rangle$ to write expectations. Specifically,

$$R^{(v)}(h) := \mathbb{E}_{\mathbf{x} \sim \mu^{(v)}} [\ell(h(\mathbf{x}), h^{(v)}(\mathbf{x}))] = \langle \ell(h, h^{(v)}), \mu^{(v)} \rangle. \quad (16)$$

From the definition of risk,

$$\begin{aligned} R^{(u)}(h) &= \langle \ell(h, h^{(u)}), \mu^{(u)} \rangle = \langle \ell(h, h^{(s)}), \mu^{(s)} \rangle - \langle \ell(h, h^{(s)}), \mu^{(s)} \rangle + \langle \ell(h, h^{(u)}), \mu^{(u)} \rangle \\ &= R^{(s)}(h) + (\langle \ell(h, h^{(u)}), \mu^{(u)} \rangle - \langle \ell(h, h^{(s)}), \mu^{(u)} \rangle) + (\langle \ell(h, h^{(s)}), \mu^{(u)} \rangle - \langle \ell(h, h^{(s)}), \mu^{(s)} \rangle) \\ &\leq R^{(s)}(h) + \langle \ell(h^{(u)}, h^{(s)}), \mu^{(u)} \rangle + \langle \ell(h, h^{(s)}), \mu^{(u)} - \mu^{(s)} \rangle \end{aligned} \quad (17)$$

where (17) follows from the triangle inequality $\ell(h, h^{(u)}) \leq \ell(h, h^{(s)}) + \ell(h^{(s)}, h^{(u)})$ and because $\ell(h^{(s)}, h^{(u)}) = \ell(h^{(u)}, h^{(s)})$.

In an analogous fashion, it is possible to show that:

$$R^{(u)}(h) \leq R^{(s)}(h) + \langle \ell(h^{(u)}, h^{(s)}), \mu^{(s)} \rangle + \langle \ell(h, h^{(u)}), \mu^{(u)} - \mu^{(s)} \rangle. \quad (18)$$

Let $\mathbf{z} = f(\mathbf{x})$. Since f is invertible, $\mathbf{x} = f^{-1}(\mathbf{z})$. The third term in the right-hand side of (18) can be bounded as follows.

$$\begin{aligned} & \langle \ell(h, h^{(u)}), \mu^{(u)} - \mu^{(s)} \rangle \\ &= \langle \ell(g \circ f, g^{(u)} \circ f^{(u)}), \mu^{(u)} - \mu^{(s)} \rangle \\ &= \mathbb{E}_{\mathbf{x} \sim \mu^{(u)}} [\ell(g \circ f(\mathbf{x}), g^{(u)} \circ f^{(u)}(\mathbf{x}))] - \mathbb{E}_{\mathbf{x} \sim \mu^{(s)}} [\ell(g \circ f(\mathbf{x}), g^{(u)} \circ f^{(u)}(\mathbf{x}))] \\ &= \mathbb{E}_{\mathbf{z} \sim f_{\#}\mu^{(u)}} [\ell(g(\mathbf{z}), g^{(u)} \circ f^{(u)} \circ f^{-1}(\mathbf{z}))] - \mathbb{E}_{\mathbf{z} \sim f_{\#}\mu^{(s)}} [\ell(g(\mathbf{z}), g^{(u)} \circ f^{(u)} \circ f^{-1}(\mathbf{z}))] \\ &= \langle \ell(g, g^{(u)} \circ f^{(u)} \circ f^{-1}), f_{\#}\mu^{(u)} - f_{\#}\mu^{(s)} \rangle \\ &\leq L \langle 1, |f_{\#}\mu^{(u)} - f_{\#}\mu^{(s)}| \rangle \end{aligned} \quad (19)$$

where (19) follows from the assumption that the loss function is bounded by a positive number L and the fact that $f_{\#}\mu^{(u)} - f_{\#}\mu^{(s)} \leq |f_{\#}\mu^{(u)} - f_{\#}\mu^{(s)}|$.

Combining (18) and (19) we get,

$$R^{(u)}(h) \leq R^{(s)}(h) + \langle \ell(h^{(u)}, h^{(s)}), \mu^{(s)} \rangle + L \langle 1, |f_{\#}\mu^{(u)} - f_{\#}\mu^{(s)}| \rangle. \quad (20)$$

By similar reasoning, from (17),

$$R^{(u)}(h) \leq R^{(s)}(h) + \langle \ell(h^{(u)}, h^{(s)}), \mu^{(u)} \rangle + L \langle 1, |f_{\#}\mu^{(u)} - f_{\#}\mu^{(s)}| \rangle. \quad (21)$$

The proof of Lemma 1 now follows by combining (20) and (21) and noting that

$$\sigma^{(u,s)} = \min \left(\langle \ell(h^{(u)}, h^{(s)}), \mu^{(u)} \rangle, \langle \ell(h^{(u)}, h^{(s)}), \mu^{(s)} \rangle \right),$$

and

$$\langle 1, |f_{\#}\mu^{(u)} - f_{\#}\mu^{(s)}| \rangle = \|f_{\#}\mu^{(u)} - f_{\#}\mu^{(s)}\|_1.$$

B.2 Extension of Proof of Lemma 1 for Nearly Invertible Representation Maps

The proof of Lemma 1 requires that the representation map f is exactly invertible. However, this restricted condition can be relaxed. In practice, a function is called nearly invertible if there exists a reconstruction function with a sufficiently low reconstruction error. Based on the definition of nearly invertible maps, we can construct an upper bound similar to the one in Lemma 1 under some additional technical conditions that are discussed in what follows.

Let the representation map f be nearly invertible, i.e., there exists a function $s : \mathbb{R}^{d'} \rightarrow \mathbb{R}^d$ such that if $f(\mathbf{x}) = \mathbf{z}$ then $\|\mathbf{x} - s(\mathbf{z})\| \leq \delta \forall \mathbf{z}$ where δ is a small positive constant. Suppose that $h^{(u)}$ is

K -Lipschitz continuous. Then, $h^{(u)}(s(\mathbf{z})) - K\delta \leq h^{(u)}(\mathbf{x}) \leq h^{(u)}(s(\mathbf{z})) + K\delta$. Further suppose that the cost function $\ell(\cdot, \cdot)$ is Q -Lipschitz continuous, i.e., $\ell(a, b) - Q|\gamma| \leq \ell(a, b + \gamma) \leq \ell(a, b) + Q|\gamma|$. Then,

$$\begin{aligned}
& \langle \ell(h, h^{(u)}), \mu^{(u)} - \mu^{(s)} \rangle \\
&= \langle \ell(g \circ f, g^{(u)} \circ f^{(u)}), \mu^{(u)} - \mu^{(s)} \rangle \\
&= \mathbb{E}_{\mathbf{x} \sim \mu^{(u)}} [\ell(g \circ f(\mathbf{x}), h^{(u)}(\mathbf{x}))] - \mathbb{E}_{\mathbf{x} \sim \mu^{(s)}} [\ell(g \circ f(\mathbf{x}), h^{(u)}(\mathbf{x}))] \\
&\leq \max \left\{ \mathbb{E}_{\mathbf{z} \sim f_{\#}\mu^{(u)}} [\ell(g(\mathbf{z}), h^{(u)}(s(\mathbf{z})) + K\delta)], \mathbb{E}_{\mathbf{z} \sim f_{\#}\mu^{(u)}} [\ell(g(\mathbf{z}), h^{(u)}(s(\mathbf{z})) - K\delta)] \right\} \\
&\quad - \min \left\{ \mathbb{E}_{\mathbf{z} \sim f_{\#}\mu^{(s)}} [\ell(g(\mathbf{z}), h^{(u)}(s(\mathbf{z})) + K\delta)], \mathbb{E}_{\mathbf{z} \sim f_{\#}\mu^{(s)}} [\ell(g(\mathbf{z}), h^{(u)}(s(\mathbf{z})) - K\delta)] \right\} \\
&\leq \mathbb{E}_{\mathbf{z} \sim f_{\#}\mu^{(u)}} [\ell(g(\mathbf{z}), g^{(u)} \circ f^{(u)}(s(\mathbf{z})))] - \mathbb{E}_{\mathbf{z} \sim f_{\#}\mu^{(s)}} [\ell(g(\mathbf{z}), g^{(u)} \circ f^{(u)}(s(\mathbf{z})))] \\
&\quad + \mathbb{E}_{\mathbf{z} \sim f_{\#}\mu^{(u)}} [QK\delta] + \mathbb{E}_{\mathbf{z} \sim f_{\#}\mu^{(s)}} [QK\delta] \\
&\leq \langle \ell(g, g^{(u)}), f_{\#}\mu^{(u)} - f_{\#}\mu^{(s)} \rangle + QK\delta + QK\delta \\
&\leq L \langle 1, |f_{\#}\mu^{(u)} - f_{\#}\mu^{(s)}| \rangle + 2QK\delta
\end{aligned} \tag{22}$$

where the fourth inequality due to the assumption that $\ell(\cdot, \cdot)$ is a distance metric, both $g(\cdot)$ and $g^{(u)}(\cdot)$ map \mathbf{z} to 1-dimension space and the fact that $h^{(u)}(s(\mathbf{z})) - K\delta \leq h^{(u)}(\mathbf{x}) \leq h^{(u)}(s(\mathbf{z})) + K\delta$, the fifth inequality due to $\ell(\cdot, \cdot)$ is Q -Lipschitz, and the last inequality due to $\ell(\cdot, \cdot)$ is bounded by L . In comparison to the original result in Lemma 1, one more term ($2QK\delta$) is introduced in the upper bound if the representation map is nearly invertible. If $\delta = 0$, $\forall \mathbf{z}$, or in other words, the representation map is exactly invertible, then the extra term $2QK\delta$ is, of course, zero.

B.3 Proof of Lemma 3

From Pinsker's inequality [Berend et al., 2014, Csiszár and Körner, 2011], the L^1 distance can be bounded by Kullback–Leibler (KL) divergence as follows:

$$\|\mu - \nu\|_1^2 \leq 2d_{KL}(\mu, \nu) \tag{23}$$

where $\|\mu - \nu\|_1$ and $d_{KL}(\mu, \nu)$ denote L^1 distance and Kullback–Leibler divergence between two distributions μ and ν , respectively. Since $\|\mu - \nu\|_1 = \|\nu - \mu\|_1$, using Pinsker's inequality for (μ, ν) and (ν, μ) ,

$$2\|\mu - \nu\|_1^2 = \|\mu - \nu\|_1^2 + \|\nu - \mu\|_1^2 \leq 2d_{KL}(\mu, \nu) + 2d_{KL}(\nu, \mu) \tag{24}$$

which is equivalent to,

$$\|\mu - \nu\|_1 \leq \sqrt{d_{KL}(\mu, \nu) + d_{KL}(\nu, \mu)}. \tag{25}$$

Next, if μ and ν are (c_1, c_2) -regular distributions, their Kullback–Leibler divergences can be bounded by their Wasserstein-2 distance as follows (please see equation (10), Proposition 1 in [Polyanskiy and Wu, 2016]),

$$d_{KL}(\mu, \nu) + d_{KL}(\nu, \mu) \leq 2 \left(\frac{c_1}{2} \sqrt{\mathbb{E}_{\mathbf{u} \sim \mu} [\|\mathbf{u}\|_2^2]} + \frac{c_1}{2} \sqrt{\mathbb{E}_{\mathbf{v} \sim \nu} [\|\mathbf{v}\|_2^2]} + c_2 \right) [\mathbf{W}_2(\mu, \nu)]. \tag{26}$$

Combining (25) and (26),

$$\|\mu - \nu\|_1 \leq \sqrt{c_1 \left(\sqrt{\mathbb{E}_{\mathbf{u} \sim \mu} [\|\mathbf{u}\|_2^2]} + \sqrt{\mathbb{E}_{\mathbf{v} \sim \nu} [\|\mathbf{v}\|_2^2]} \right)} + 2c_2 [\mathbf{W}_2(\mu, \nu)]^{1/2}. \quad (27)$$

B.4 Proof of Theorem 1

Under the assumption that $f_{\#}\mu^{(s)}$ and $f_{\#}\mu^{(u)}$ are (c_1, c_2) -regular $\forall s = 1, 2, \dots, S$, from Lemma 3,

$$\begin{aligned} \|f_{\#}\mu^{(u)} - f_{\#}\mu^{(s)}\|_1 &\leq \sqrt{c_1 \left(\sqrt{\mathbb{E}_{\mathbf{x} \sim \mu^{(s)}} [\|f(\mathbf{x})\|_2^2]} + \sqrt{\mathbb{E}_{\mathbf{x} \sim \mu^{(u)}} [\|f(\mathbf{x})\|_2^2]} \right)} + 2c_2 \\ &\quad \times [\mathbf{W}_2(f_{\#}\mu^{(u)}, f_{\#}\mu^{(s)})]^{1/2}. \end{aligned} \quad (28)$$

Let:

$$C := \max_{s \in \{1, \dots, S\}} \sqrt{c_1 \left(\sqrt{\mathbb{E}_{\mathbf{x} \sim \mu^{(s)}} [\|f(\mathbf{x})\|_2^2]} + \sqrt{\mathbb{E}_{\mathbf{x} \sim \mu^{(u)}} [\|f(\mathbf{x})\|_2^2]} \right)} + 2c_2. \quad (29)$$

Multiplying (28) by $\lambda^{(s)}$ and summing over all s we get:

$$\sum_{s=1}^S \lambda^{(s)} \|f_{\#}\mu^{(u)} - f_{\#}\mu^{(s)}\|_1 \leq C \sum_{s=1}^S \lambda^{(s)} [\mathbf{W}_2(f_{\#}\mu^{(u)}, f_{\#}\mu^{(s)})]^{1/2}. \quad (30)$$

By Jensen's inequality,

$$\sum_{s=1}^S \lambda^{(s)} [\mathbf{W}_2(f_{\#}\mu^{(u)}, f_{\#}\mu^{(s)})]^{1/2} \leq \left[\sum_{s=1}^S \lambda^{(s)} \mathbf{W}_2^2(f_{\#}\mu^{(u)}, f_{\#}\mu^{(s)}) \right]^{1/4}. \quad (31)$$

From (30) and (31),

$$\sum_{s=1}^S \lambda^{(s)} \|f_{\#}\mu^{(u)} - f_{\#}\mu^{(s)}\|_1 \leq C \left[\sum_{s=1}^S \lambda^{(s)} \mathbf{W}_2^2(f_{\#}\mu^{(u)}, f_{\#}\mu^{(s)}) \right]^{1/4}. \quad (32)$$

Finally, combining the upper bound in Lemma 2 and (32), the proof follows.

B.5 Proof of Corollary 1

We begin with the second term in the upper bound of Theorem 1. For any arbitrary pushforward distribution $f_{\#}\mu$, we have:

$$\left[\sum_{s=1}^S \lambda^{(s)} \mathbf{W}_2^2(f_{\#}\mu^{(u)}, f_{\#}\mu^{(s)}) \right]^{1/4} \quad (33)$$

$$\leq \left[\sum_{s=1}^S \lambda^{(s)} \left(\mathbf{W}_2^2(f_{\#}\mu^{(u)}, f_{\#}\mu) + \mathbf{W}_2^2(f_{\#}\mu, f_{\#}\mu^{(s)}) \right) \right]^{1/4} \quad (34)$$

$$= \left[\sum_{s=1}^S \lambda^{(s)} \mathbf{W}_2^2(f_{\#}\mu^{(u)}, f_{\#}\mu) + \sum_{s=1}^S \lambda^{(s)} \mathbf{W}_2^2(f_{\#}\mu, f_{\#}\mu^{(s)}) \right]^{1/4} \quad (35)$$

$$= \left[\mathbf{W}_2^2(f_{\#}\mu^{(u)}, f_{\#}\mu) + \sum_{s=1}^S \lambda^{(s)} \mathbf{W}_2^2(f_{\#}\mu, f_{\#}\mu^{(s)}) \right]^{1/4} \quad (36)$$

$$\leq \left[\sum_{s=1}^S \lambda^{(s)} \mathbf{W}_2^2(f_{\#}\mu, f_{\#}\mu^{(s)}) \right]^{1/4} + \left[\mathbf{W}_2^2(f_{\#}\mu^{(u)}, f_{\#}\mu) \right]^{1/4} \quad (37)$$

with (34) due to the triangle inequality, (36) due to $\sum_{s=1}^S \lambda^{(s)} = 1$, (37) due to the fact that for any $a, b \geq 0$ and $0 < p \leq 1$, $(a + b)^p \leq a^p + b^p$.

C ARCHITECTURE AND HYPE-PARAMETERS

Model structure for decoder can be found in Table 4 and a list of all hyper-parameters of the proposed methods is shown in Table 5

Table 4: Decoder model structure for WBAE

Layer
Linear (in=200, out=512) + BatchNorm + ReLU
Linear (in=512, out=2048) + BatchNorm + ReLU
ConvTranspose2d (in_channel=32, out_channel=16, kernel_size=3, stride= 2)
BatchNorm2d + ReLU
ConvTranspose2d (in_channel=16, out_channel=8, kernel_size=5, stride=2)
BatchNorm2d + ReLU
ConvTranspose2d (in_channel=8, out_channel=3, kernel_size=5, stride=3)
BatchNorm2d + ReLU
Interpolate (size=(224, 224))

Table 5: Hyper-parameters of the proposed methods and the search sets

Parameters	Value
learning rate	0.00005
batch size	32
ResNet dropout	0
weight decay	0
epoch	40
δ	0.1
ϵ	0.5
α	{0.0001, 0.0005}
β	{0.0001, 0.0005, 0.001, 0.005}